Commun. Comput. Phys.
doi: 10.4208/cicp.100510.150511s

Vol. **11**, No. 4, pp. 1081-1102
April 2012

REVIEW ARTICLE

High-Order and High Accurate CFD Methods and Their Applications for Complex Grid Problems

Xiaogang Deng*, Meiliang Mao, Guohua Tu, Hanxin Zhang and Yifeng Zhang

State Key Laboratory of Aerodynamics, Aerodynamics Research & Development Center, Mianyang, 621000, P.R. China.

Received 15 May 2010; Accepted (in revised version) 15 May 2011

Available online 29 November 2011

Abstract. The purpose of this article is to summarize our recent progress in high-order and high accurate CFD methods for flow problems with complex grids as well as to discuss the engineering prospects in using these methods. Despite the rapid development of high-order algorithms in CFD, the applications of high-order and high accurate methods on complex configurations are still limited. One of the main reasons which hinder the widely applications of these methods is the complexity of grids. Many aspects which can be neglected for low-order schemes must be treated carefully for high-order ones when the configurations are complex. In order to implement high-order finite difference schemes on complex multi-block grids, the geometric conservation law and block-interface conditions are discussed. A conservative metric method is applied to calculate the grid derivatives, and a characteristic-based interface condition is employed to fulfil high-order multi-block computing. The fifth-order WCNS-E-5 proposed by Deng [9, 10] is applied to simulate flows with complex grids, including a double-delta wing, a transonic airplane configuration, and a hypersonic X-38 configuration. The results in this paper and the references show pleasant prospects in engineering-oriented applications of high-order schemes.

AMS subject classifications: 76M20

Key words: WCNS, complex configurations, geometric conservation law, conservative metric methods, characteristic-based interface conditions.

Contents

*Corresponding author. *Email addresses:* `xgdeng@skla.cardc.cn` (X. Deng), `mlmao@skla.cardc.cn` (M. Mao), `ghtu@skla.cardc.cn` (G. Tu), `hxzhang@skla.cardc.cn` (H. Zhang), `yfzhang@skla.cardc.cn` (Y. Zhang)

1 Introduction

Over the past 20 to 30 years, there have been a lot of studies in developing and applying high-order and high accurate numerical methods for computational fluid dynamics (CFD). Although low-order schemes (second-order schemes) are widely used for engineering applications, they are insufficient for turbulence, aeroacoustics, and many viscosity dominant flows, such as boundary layer flows, vortical flows, shock-boundary layer interactions, heat flux transfers, etc. An effective approach to overcome the obstacle of accurate numerical simulations is to employ high-order methods [1]. In [2, 3], Shu and Cheng gave profound reviews on high-order weighted essentially non-oscillatory (WENO) schemes and discontinuous Galerkin (DG) schemes. A comprehensive review was also given by Ekaterinaris [4] for high-order difference schemes, ENO and WENO schemes, DG schemes, and spectral volume (SV) schemes.

It is generally believed that the accurate simulation of fluid flow with multiple and wide range of spatial scales and structures is a difficult task except through spectral approximations. However, the use of spectral approximations is limited to simple geometries with generally periodic boundary conditions. Compact schemes make it possible to devise, on a given stencil, finite difference schemes that have much better resolution properties than conventional explicit finite difference schemes of comparable order of accurate. Compact schemes with spectral-like resolution properties are more convenient to use than spectral and pseudo-spectral schemes, and are easier to handle, especially when nontrivial geometries are involved [5]. Deng et al. [6] have proposed a type of one-parameter linear dissipative compact schemes (DCS). DCSs are derived for high-order accurate simulation of shock-free problems while damping out the dispersive and parasite errors in the high-wave-number regions. Visbal and Gaitonde [7] use filters to prevent numerical oscillations of central compact schemes. In order to dealing with shock wave problems, Adams and Shariff [74] have developed a compact-ENO scheme. Pirozzoli [75] have developed a compact-WENO scheme which was further improved by Ren et al. [73]. Deng et al. have developed compact nonlinear schemes [8] and weighted compact nonlinear schemes (WCNS) [9, 10]. The WCNSs have been successfully applied to a wide range of flow simulations so far to show its flexibility and robustness [11, 16, 32, 99, 100]. Some results on using the fifth-order WCNS (WCNS-E-5) [9, 10] for complex grid problems are presented in this paper to further show its engineering prospects.

2 High-order and high accurate CFD methods for complex grid problems

The state-of-the-art applications of high-order and high-accurate methods in complex grids are still limited, while there are many kinds of high-order schemes, such as compact schemes [5–7,33,35], WCNSs [9,10], ENO [37,38] and WENO schemes [2,3,39,52,53], DG schemes [40–44,48,49,51,54], spectral methods (including spectral element (SE) [55], SV [56,57,110], spectral difference (SD) [58], staggered spectral methods [60]), gas-kinetic schemes (GKS) [61,63–65], dispersion-relation-preserving (DRP) schemes [67], low dissipative high-order schemes [68], monotonicity preserving (MP) schemes [69,70], group velocity control (GVC) schemes [71,72], SPH methods [45,62], ALE methods [64–66,81], methods for multiphase flows [42,46,47], and many hybrid ones [73–76]. In most published articles and reviews, the flows are complex with shock waves, vortices, and turbulent structures, while the grids are relatively simple. Despite many authors say in their articles that they have successfully applied high-order schemes in complex geometries, the grids in their test cases are still very simple when compared to those frequently appear in low-order scheme applications. Taking WENO schemes for example, as one of the most widely popularized high-order schemes, there are hundreds of articles on WENO schemes or employing WENO schemes for complex flows. However, It is not easy to find a grid or configuration which can compare with the complexity of any grids or configurations applied in the four series of AIAA CFD Drag Prediction Workshops (DPW, DPW I $\sim$ DPW IV) [77].

Although the finite volume methods (FVM), the finite element methods (FEM) and the DG schemes with unstructured grid system have advantages in treating complex geometries, the finite difference methods (FDM) with the structured grid system are superior in boundary layer simulations, computing costs, and convenience. Thus high-order multi-block FDM techniques are still attractive at present and in the future. Perhaps, many undesirable effects will not occur or can be neglected for lower-order methods, but they should be considered carefully for high-order methods. The interface conditions for multi-block grids, geometric conservation law (GCL), viscous treatments and convergence accelerating are some of such factors that must be reevaluated for high-order schemes.

Generally speaking, it is difficult to generate a high-quality structured single-block grid system for a complex configuration. Visbal and Gaitonde [7,13], Delfs [14], Sherer et al. [15] and many other researchers use overset grid strategy for high-order FDM. However, the inherent interpolations in overset grids may cause numerical instability and loss of global accuracy, especially when there are shock waves. Furthermore, the grid topologies and numerical procedures for overset grid approach are generally complicated and not easy to implement for 3D complex configurations. Point-matched multi-block structured grids, or patched grids, which do not require overlapped zones, are widely adopted choices for complex configurations. Multi-block structured grid technique makes it possible to run high-order finite difference schemes on each individual block, and the information transmission between neighbouring blocks and the propagation throughout the flow field can be realized by some kinds of interface conditions. Rai [17] used a flux interpolation to construct coupled conditions on mid-node with Beam-Warming and Osher scheme. Lerat and Wu [18] adopted local flux construction to establish conservative and unconditionally stable interface conditions. Huan, Hicken and Zingg [19, 20] proposed a kind of high-order interface boundary schemes which combine a conventional scheme and a summation-by-parts (SBP) [21–23] scheme with simultaneous approximation terms (SATs) [24–26]. The SBP operators are derived from the energy method, first by Kreiss and Scherer in 1974 [21] for low orders, and extended to high-order by Strand [27] and Jurgens [28]. The SBP operators allow an energy estimate of the discrete form, potentially guaranteeing strict stability for hyperbolic problems. However, boundary operators are needed, which can destroy the SBP property [22]. With the aim of preserving the SBP property of the overall scheme, the projection method [23] and the SAT approach [24] have been developed. However, the projection method becomes unstable for the linear convection-diffusion equation despite that it is strictly stable for hyperbolic PDEs [22]. Then, this kind of interface method is mainly adopted in linear hyperbolic systems and further improvement and examinations are necessary to upgrade this kind of interface boundary schemes suitable for fluids dynamics (Navier-Stokes systems). In content of CFD, Kim and Lee [29] and Sumi et al. [12, 30, 31] employed characteristic interface conditions (CIC) or generalized characteristic interface conditions (GCIC) which show some attractive performance in practice. We have derived some new interface approaches (CBIC) which directly exchange the spatial derivatives (i.e. RHS, computed on each block) on each side of an interface by means of a characteristic-based projection [32]. The CBIC have shown excellent performance in complex grids.

Traditionally, high-order FDM require smooth grids, and the smoothness of the grids shall be comparable with the order of the accuracy of the schemes [3]. This premise is usually far more rigorous for complex configurations even when multi-block decomposition techniques are applied. One may feel despair on using high-order methods for complex configurations after reading the comments above. Fortunately, Visbal and Gaitonde [78] have shown that high-order schemes can be applied in low quality grids such as extremity deforming grids and nondifferentiable grids if some special techniques are applied to get rids of the GCL-related errors and numerical oscillations. The studies of Visbal et al. [78] and Nonomura et al. [79] indicate that the GCL is very important in ensuring freestream preservation. Our experiences show that low quality grids bear large GCL-related errors than that of high-quality grids. A general condition to satisfy the GCL in FDM has been derived by Deng et al. [100].

High-order accuracy requires high-order evaluations for both the inviscid and viscous terms. However, most efforts, including many in the references mentioned above, mainly focus on the inviscid terms to resolve discontinuities and small scale structures. In order to supplement 5th-order WENO scheme with high-order viscous formula, Shen et al. [101] developed a 4th-order conservative scheme with the stencil less than that of the WENO scheme. Deng [10] listed some viscous derivative and interpolation formulas for WCNSs. Tu et al. [94] proposed a staggered compact difference scheme to avoid the odd-even oscillations which may emerge when high-order schemes are used. High-order viscous flux discretizations are also very important for DG, SE, SV and SD. Sun et al. [105] employed the local DG (LDG) approach in their SV method to discretize viscous terms. A penalty-like method, which is more symmetrical than LDG and better suitable for unstructured and non-uniform grids, was developed by Kannan and Wang [102] by applying the penalty method of Bassi and Rebay [87, 88]. Kannan and Wang [102] also conducted some Fourier analysis and accuracy studies for a variety of viscous flux formulations and showed that the penalizing schemes may enhance fidelity. Very recently, Kannan and Wang [103, 104] implemented the SV method for the Navier-Stokes equations using the LDG2 (which is an improvised variant of the LDG approach) [103] and the direct DG approaches [104]. However, the researches on viscous terms are still limited, and many aspects, such as stability and conservation, are still need to be further investigated for high-order and high accurate methods.

It is commonly encountered that the convergence property of high-order methods is general inferior to that of low-order methods especially when the grid quality is low. Kitamura et al. [59] employed the preconditioned LU-SGS for low speeds flows. Zhang et al. [106] investigated several implicit time matching methods, including lower-upper symmetric Gauss-Seidel (LU-SGS), generalized minimum residual (GMRES), Gauss-Seidel method with point relaxation and line relaxation. The results indicate that GMRES can considerably improve the convergence rate of WCNSs for the flows they simulated. Implicit LU-SGS is also successfully used for SD and SV, such as the methods in [107, 108]. P-multigrid approach, where p is the order of polynomial degree, is widely employed in DG [111,112], SV [108], SD [113], SE [114], and some similar schemes to accelerate convergence rate. It is worth to note that Kannan et al. [107, 108, 113] have successfully blended p-multigrid approach with pre-conditions or implicit LU-SGS, and the convergence rate is drastically improved for bad and skewed unstructured grids. For more details about p-multigrid methods, please refer to [108, 111–114] and the references therein.

3 Governing equations and the fifth-order weighted compact nonlinear scheme

In Cartesian coordinates the governing equations (Euler or Navier-Stokes) in strong conservative form are

$$\frac{\partial Q}{\partial t}+\frac{\partial F}{\partial x}+\frac{\partial G}{\partial y}+\frac{\partial H}{\partial z}=0. \tag{3.1}$$

The equations are transformed into curvilinear coordinates by introducing the transformation $(x,y,z,t)\to(\xi,\eta,\zeta,\tau)$

$$\frac{\partial \tilde{Q}}{\partial \tau}+\frac{\partial \tilde{F}}{\partial \xi}+\frac{\partial \tilde{G}}{\partial \eta}+\frac{\partial \tilde{H}}{\partial \zeta}=0, \tag{3.2}$$

where

$$\tilde{F}=\tilde{\xi}_t Q+\tilde{\xi}_x F+\tilde{\xi}_y G+\tilde{\xi}_z H, \qquad \tilde{\xi}_x=J^{-1}\xi_x,$$

and with similar relations for the other terms.

Let us first consider the discretization of the inviscid flux derivative along the ξ direction. The discretization for other inviscid fluxes can be computed by similar procedures. Suppose $U_i=U(\xi_i,t)$ be the flow variables, the fifth-order weighted compact nonlinear scheme (WCNS-E-5) can be expressed as

$$\frac{\partial \tilde{F}_i}{\partial \xi}=\frac{75}{64h}(\tilde{F}_{i+1/2}-\tilde{F}_{i-1/2})-\frac{25}{384h}(\tilde{F}_{i+3/2}-\tilde{F}_{i-3/2})+\frac{3}{640h}(\tilde{F}_{i+5/2}-\tilde{F}_{i-5/2}), \tag{3.3}$$

where h is the grid size, and

$$\tilde{F}_{i+1/2}=\tilde{F}\left(U^L_{i+1/2},U^R_{i+1/2},\tilde{\xi}_{x,i+1/2},\tilde{\xi}_{y,i+1/2},\tilde{\xi}_{z,i+1/2}\right) \tag{3.4}$$

is computed by some kind of flux-splitting method which can be found in [9]. $U^L_{i+1/2}$ and $U^R_{i+1/2}$ are the left-hand and right-hand cell-edge flow variables, which are obtained by a high-order nonlinear weighted interpolation. The idea is that the stencil to interpolate the cell-edge values contains several substencils, each of the substencils is assigned a weight factor, which determines its contribution to the final approximation of the cell-edge values. The weights are designed in such a way that in the smooth region they approach the optimal weights to achieve fifth-order accuracy, whereas in the regions near the discontinuities, the weight of the substencil, which contains the discontinuities, is assigned nearly zero. Therefore the weighted interpolations can prevent numerical oscillations around discontinuities. For more details, see, [9,10].

4 Geometric conservative law and the conservative metric method

The concept of the geometric conservative law (GCL) was first introduced in 1961 by Trulio and Trigger [80]. In 1978, Pulliam & Steger [84] observed that the metric discretizations will lead to the nonconservation of flow fields. Thomas & Lombard [85] extended the conception of the GCL to general applications in CFD. The effect of the GCL can be evidently noted in finite difference system when curvilinear coordinate transformation is applied. Eqs. (3.2) is equivalent to (3.1) only if the following GCL items are all zero.

$$I_t=(1/J)_\tau+(\tilde{\xi}_t)_\xi+(\tilde{\eta}_t)_\eta+(\tilde{\zeta}_t)_\zeta, \tag{4.1}$$

$$I_x=(\tilde{\xi}_x)_\xi+(\tilde{\eta}_x)_\eta+(\tilde{\zeta}_x)_\zeta, \quad I_y=(\tilde{\xi}_y)_\xi+(\tilde{\eta}_y)_\eta+(\tilde{\zeta}_y)_\zeta, \quad I_z=(\tilde{\xi}_z)_\xi+(\tilde{\eta}_z)_\eta+(\tilde{\zeta}_z)_\zeta. \tag{4.2}$$

The first item (I_t) constitutes a differential statement of volume conservation, and I_x, I_y and I_z express surface conservation. The GCL usually is divided into the volume conservation law (VCL) and the surface conservation law (SCL) as discussed by Zhang et al. [93]. In fact, $I_t = I_x = I_y = I_z = 0$ analytically provided that the grids are differentiable. However, it may not be true in discretized forms because of numerical errors. Even when low-order schemes are used, Étienne et al. [86] showed that a numerical method satisfying the VCL will generally allow a much larger computational time step than its counterpart violating the VCL. To ensure the VCL, the volume conservation item is usually applied to calculate the time derivative of Jacobian following

$$(1/J)_\tau = -[(\tilde{\xi}_t)_\xi + (\tilde{\eta}_t)_\eta + (\tilde{\zeta}_t)_\zeta]$$

by many authors [78, 86]. The errors in I_x, I_y and I_z are usually related to grid quality, such as smoothness, uniformity, orthogonality, and stretch rate. High-order schemes with their low dissipative property usually bear more risk from the SCL-related errors than that of low-order schemes. This difficult is one of the key obstacles which hinder the widely applications of high-order schemes for complex grid problems. In order to use high-order schemes for low quality grids, a conservative metric method (CMM) which can ensure the SCL has been derived by Deng et al. [100]. The CMM contains the following two aspects:

(i) First, the metrics are acquired through the 'conservative forms'

$$\tilde{\xi}_x = (y_\eta z)_\zeta - (y_\zeta z)_\eta, \quad \tilde{\eta}_x = (y_\zeta z)_\xi - (y_\xi z)_\zeta, \quad \tilde{\zeta}_x = (y_\xi z)_\eta - (y_\eta z)_\xi \tag{4.3}$$

and with similar relations for the remain items.

(ii) Second, for each grid (coordinate) direction, the algorithm for the derivatives in Eq. (4.3) shall be identical to that of flow fluxes where the metrics are re-discretized in combination with the flow fluxes.

When the flux derivatives are discretized, the metrics are re-discretized because that the fluxes contain metrics. Then we can get equivalent schemes for the re-discretizations of the metrics. The equivalent schemes are called the re-discretization schemes in this paper. For WCNS-E-5, the re-discretization scheme is

$$\frac{\partial a_i}{\partial \xi} = \frac{75}{64h}[a_{i+1/2} - a_{i-1/2}] - \frac{25}{384h}[a_{i+3/2} - a_{i-3/2}] + \frac{3}{640h}[a_{i+5/2} - a_{i-5/2}], \tag{4.4}$$

where the cell-edge values can be acquired by high-order linear interpolations. In this paper, we use

$$a_{i+1/2} = \frac{1}{16}(-a_{i-1} + 9a_i + 9a_{i+1} - a_{i+2}). \tag{4.5}$$

5 Characteristic-based interface conditions

Characteristic boundary conditions have been widely studied by many researchers, such as Thompson [89] and Poinsot and Lele [90]. Characteristic interface conditions for multi-block grids have also been studied by Kim and Lee [29], Sumi et al. [30, 31] and

Deng et al. [32]. The characteristic-based interface condition (CBIC), which was developed by Deng et al. [32], will be briefly introduced below.

Defining the transformation matrix P_{QV_C} in terms of conservative variables Q, and characteristic variables V_C,

$$P_{QV_C} = \frac{\partial Q}{\partial V_C}. \tag{5.1}$$

Let

$$RHS = -J\left(\frac{\partial \tilde{F}}{\partial \xi} + \frac{\partial \tilde{G}}{\partial \eta} + \frac{\partial \tilde{H}}{\partial \zeta}\right). \tag{5.2}$$

The characteristic-based interface conditions (CBIC) are

$$\left\{\begin{array}{l} \left.\dfrac{\partial Q}{\partial t}\right|_L = \left(A_s^+\right)\big|_L (RHS)|_L + \left(A_s^-\right)\big|_L (RHS)|_R, \\ \left.\dfrac{\partial Q}{\partial t}\right|_R = \left(A_s^+\right)\big|_R (RHS)|_R + \left(A_s^-\right)\big|_R (RHS)|_L, \end{array}\right. \tag{5.3}$$

where

$$A_s^+ = P_{QVc} diag\left[(1+sign(\lambda_i))/2\right] P_{QVc}^{-1}, \quad A_s^- = P_{QVc} diag\left[(1-sign(\lambda_i))/2\right] P_{QVc}^{-1},$$

$(A_s^+)|_{L,R}$ are calculated by the variables on the interface, and $(RHS)|_{L,R}$ can be calculated by one-side differencing or other methods. Here, the subscripts, "L" and "R" denote the variables and terms on an interface but belong to the left-hand-side sub-block and the right-hand-side sub-block, respectively. One can verify that $(\partial Q/\partial t)|_L = (\partial Q/\partial t)|_R$. Please refer to [32] for more details about the CBIC, such as the implementations.

6 Applications and discussions

6.1 A hypersonic cylinder problem with interfaces on the shock wave

The effectiveness of the CBIC has been shown for a wide range of flows except shock waves by Deng et al. [32]. This case is chosen to show that the CBIC works well across shock waves provided that the RHS_L and RHS_R are oscillation-free. The flow is supposed to be laminar, and the incoming flow conditions for computing are: $Ma = 8.03$, $Re = 1.835\times 10^5$, $T_\infty = 124.94$K, $T_w = 294.44$K, and the minimal grid size $h_{min} = 20/Re$.

The whole computed domain (121×81 notes) is decomposed into 7 sub-domains which are shown in Fig. 1. Three interfaces with a triple connecting point and a quadruple connecting point are purposively set on the static shock wave to check performances of the CBIC. Although the flow field is relatively simple, it is a tough case for an interface management technique because the strong shock wave will not only cross some of the interfaces, but also settle on some other interfaces ultimately. The computation begins at the uniform inflow conditions, then the shock wave first forms at the solid wall and then

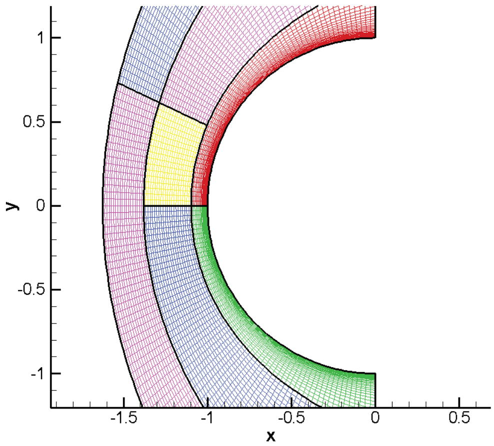

Figure 1: The grids over the cylinder.

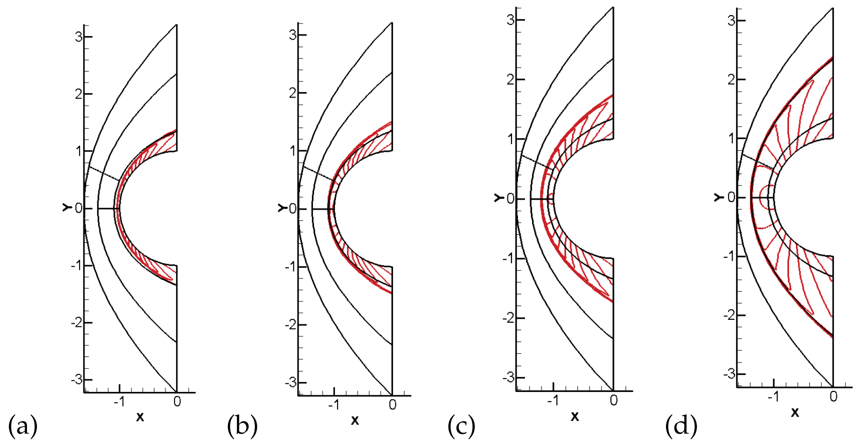

Figure 2: The bow shock wave at different computational moment, pressure contours.

marches its way to the final position. Fig. 2(a) shows pressure contours at the moment when the shock wave is near the wall. Fig. 2(b) shows result at the moment when the shock wave is traversing the first three interfaces which are 'parallel' to the wall. Fig. 2(c) shows the result at the moment after the shock wave successfully traversed the first three wall-parallel interfaces. Fig. 2(d) shows the finial computed result with the shock wave settles on the other three wall-parallel interfaces. Although the decomposed domains are asymmetric to the y-axis, the result shown in Fig. 2 is still symmetric. Fig. 3 shows the enlarged views at two of the triple connecting points and one of the quadruple connecting points. It can be seen that the results are smooth as if there are no interfaces. The wall pressure distribution and wall heat transfer rate distribution are shown in Fig. 4, which shows that the computed results are consistent with the experimental results of Wieting [95].

DOI https://doi.org/10.4208/cicp.100510.150511s | Generated on 2024-12-19 01:07:36

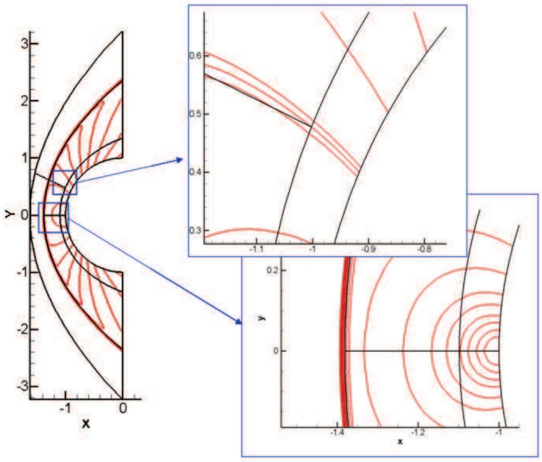

Figure 3: The enlarged parts at multi-connected points, pressure contours.

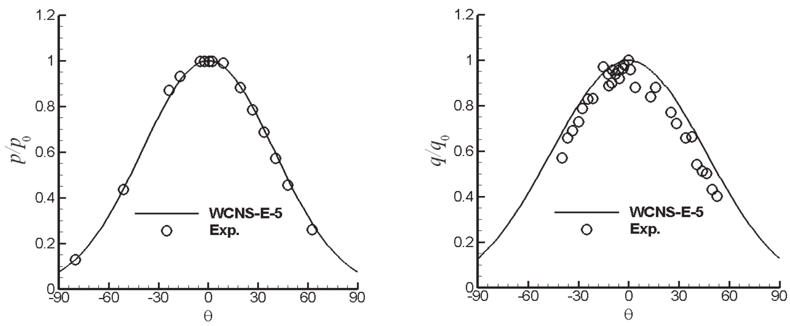

(a) Pressure (b) Heat transfer rate

Figure 4: The wall pressure and heat transfer rate.

6.2 The GCL for a blunt configuration

A two-dimensional blunt configuration with dual backward-facing steps is shown in Fig. 5(a). The flows conditions is set to be the same as that of [100], namely, $Ma = 0.3$, $Re = 2.7 \times 10^6$ (base on the height of one step), and $T_\infty = 300$K. The solid wall is assumed to be adiabatic. The flow is supposed to be full turbulence and the Spalart-Allmaras turbulence model [91] is applied here.

Although it is a two-dimensional problem, the mesh is deemed as a three-dimensional one by equally extending five grid levels in the transverse (z) direction. Before starting the simulation, a numerical analysis of the three SCL items of the GCL, namely I_x, I_y and I_z, is given to show the effectiveness of the CMM. Table 1 lists the SCL-related errors (the violation of the SCL), where N is the total grid number. Five schemes are tested here to check the characteristics of the CMM. The five schemes are the second-order explicit

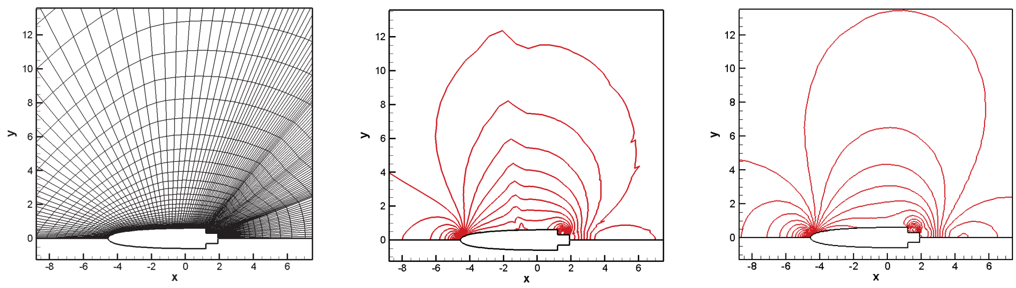

(a) (b) (c)

Figure 5: Grids and pressure contours. The flow fluxes are solved by WCNS-E-5. Middle: The metrics are solved by the traditional standard metrics of (6.1). Right: The metrics are solved by the CMM.

central scheme (EC2), the forth-order explicit central scheme (EC4), the forth-order Padé-type central compact scheme (CC4), the sixth-order Padé-type central compact scheme (CC6), and the scheme defined by Eq. (4.4) and Eq. (4.5) (WCNS-E-5). Table 1 indicates that the violation of the SCL is negligible if the CMM is applied. However, it can be seen from Table 2 that, if the schemes for the metrics are different from the re-discretization schemes for the grid-related items, the metric cancellation errors are much greater than those with the CMM, despite that the 'conservative forms' of Eqs. (4.3) are applied here. Another case is that the schemes for the metrics are same to the re-discretization schemes for the grid-related items, while the metrics are calculated by the traditional standard metric method. The errors shown in Table 3 are larger than that in Table 1. We note here that the traditional standard metrics are referred as followings

$$\tilde{\xi}_x = J^{-1}\xi_x = y_\eta z_\zeta - z_\eta y_\zeta, \quad \tilde{\eta}_x = J^{-1}\eta_x = y_\zeta z_\xi - z_\zeta y_\xi, \quad \tilde{\zeta}_x = J^{-1}\zeta_x = y_\xi z_\eta - z_\xi y_\eta, \ \cdots. \tag{6.1}$$

Table 1: I_x, I_y and I_z calculated by the CMM with different schemes.

	EC2	EC4	CC4	CC6	WCNS-E-5
$\frac{1}{N}\sum\lvert I_x\rvert$	1.14E-18	9.63E-17	1.56E-16	2.16E-16	2.04E-16
$\frac{1}{N}\sum\lvert I_y\rvert$	1.96E-17	2.39E-16	1.88E-16	5.93E-16	9.47E-16
$\frac{1}{N}\sum\lvert I_z\rvert$	8.51E-17	6.28E-16	6.58E-16	1.26E-15	1.28E-15
$\max(\lvert I_x\rvert,\lvert I_y\rvert,\lvert I_z\rvert)$	5.20E-14	2.88E-13	2.43E-13	3.74E-13	1.71E-13

Table 2: The maximal errors of I_x, I_y and I_z computed by different schemes with the conservative form (4.3).

		δ_1 schemes				
		EC2	EC4	CC4	CC6	WCNS-E-5
δ_2 schemes	ECS2	5.20E-14	2.42E-02	2.99E-02	3.84E-02	1.90E-02
	ECS4	2.42E-02	2.88E-13	2.33E-02	2.70E-02	1.89E-02
	CCS4	2.99E-02	2.33E-02	2.43E-13	1.44E-02	1.18E-02
	CCS6	3.84E-02	2.70E-02	1.44E-02	3.74E-13	2.51E-02
	WCNS-E-5	1.90E-02	1.89E-02	1.18E-02	2.51E-02	1.71E-13

Table 3: Same schemes applied both to the metrics and their re-discretization with the traditional standard metrics (6.1).

	EC2	EC4	CC4	CC6	WCNS-E-5
$\frac{1}{N}\sum\vert I_x\vert$	1.82E-16	1.24E-14	1.06E-14	1.89E-14	1.03E-15
$\frac{1}{N}\sum\vert I_y\vert$	1.01E-16	6.60E-16	6.04E-16	1.28E-15	1.15E-15
$\frac{1}{N}\sum\vert I_z\vert$	3.63E-12	1.50E-12	1.31E-12	2.06E-12	8.23E-13
$\max(\vert I_x\vert,\vert I_y\vert,\vert I_z\vert)$	8.03E-10	7.52E-10	4.33E-10	8.02E-10	2.11E-10

Our previous study shows that high-order traditional standard metric methods (CC6, [100]) may cause numerical oscillations when we conduct high-order flow computing. In this paper, we can find that the oscillations are still obvious (Fig. 5(b)) even when the metrics are calculated by the 2nd-order scheme (EC2) through the traditional standard form of Eq. (6.1). We have proved in [100] that this kind of oscillations can be successfully avoided by applying the CMM notwithstanding that the high-order schemes are applied. The result in [100] is also quoted as Fig. 5(c).

6.3 The application of the GCL for vortex preservation

A vortex convecting problem is chosen to show the performance of the GCL on vortex preservation property of high-order schemes. Similar researches can be found in Nonomura's work [79]. The initial conditions are defined by adding a vortex in a mean flow [90].The mesh contains random perturbations from a normal Cartesian grid as shown in Fig. 6(a). A nominal 50×50 uniform mesh is generated in the domain $x\in[-6,6]$, $y\in[-6,6]$. Interior points are then perturbed by 20% of the nominal spacing in a randomly chosen direction. In order to simplify the boundary treatment, four points near the boundaries of each grid line are left unperturbed. There are no analytical metric derivatives because of the discontinuities of the grid. The quality of the mesh is far lower to meet the requirements of many spatial schemes if the GCL is not satisfied during computing. For example, Visbal & Gaitonde [78] showed that the CC4 scheme and the EC4 scheme were unstable even at extremely small time steps, and strong filters are necessary to stabilize the computing. Nonomura [79] employs the same method as the CMM to calculate the metrics except that Nonomura adopts a six-order interpolation other than the forth-order interpolation (Eq. (4.5)). Nonomura's results and ours show that a vital aspect for the accurate and stable simulations of flows on this extremely lower quality grid is the SCL (namely the GCL of stationary grids). This conclusion can be easily obtained by comparing the results in Figs. 6(b), 6(c) and 6(d) in which the results at $t=12$ are shown. The CMM, which satisfies the SCL, is much superior to the traditional standard metrics in the condition of lower quality grids. If the SCL is satisfied on every discrete point, the WCNS-E-5 with its nonlinear mechanism can successfully damp out the numerical oscillations on the low quality mesh without any other extra treatments such as filters.

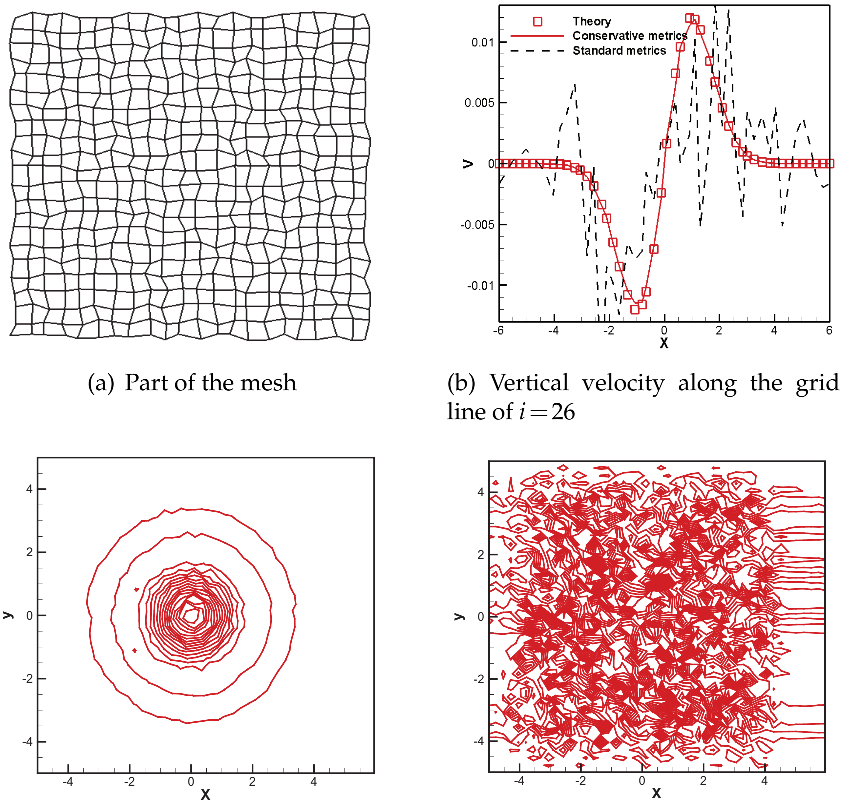

(a) Part of the mesh

(b) Vertical velocity along the grid line of $i=26$

(c) Vorticity magnitude contours with the CMM

(d) Vorticity magnitude contours with the standard metrics

Figure 6: Performance of the CMM on a randomized mesh.

6.4 Applications of the high-order WCNS-E-5 to complex grid problems

The latest CFD progresses, which include some complex applications of high-order schemes (referred as high resolution schemes by Fujii), such as linear compact schemes, WENO, and WCNS, has been summarized by in [96, 97]. Fujii et al. [16] also found that the WCNS resolves flow structure with 8-10 points per wave, and has 2-4 times higher spatial resolution than the conventional second-order TVD scheme for the simulation of acoustics from supersonic jets. The WCNS reduce the total number of grid points 10-50 times in three dimensions, which saves the same order of computer time. The applications of WCNS for implicit large eddy simulations of turbulence are tested by Ishiko et al. [98]. One aim of our studies is to apply the WCNS-E-5 to flows over complex configurations. Deng et al. [32] have successfully applied the WCNS-E-5 in simulating the complex flows over a two-element NLR7301 airfoil, a three-element 30P-30N airfoil, and a three-dimensional wing-body configuration. The followings continue to show some engineering-oriented applications of the WCNS-E-5.

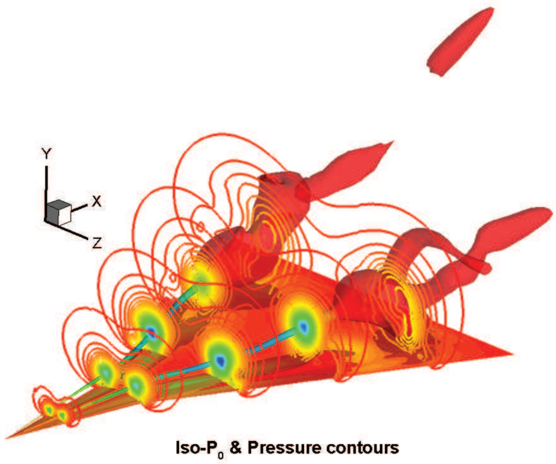

Figure 7: Iso-p_0 and pressure contours of a $Ma=0.3$ double-delta wing, 4.26 million grids.

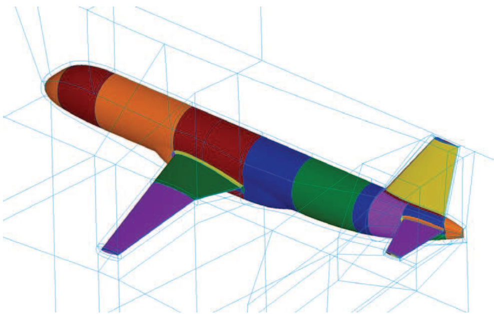

(a) Gird skeleton

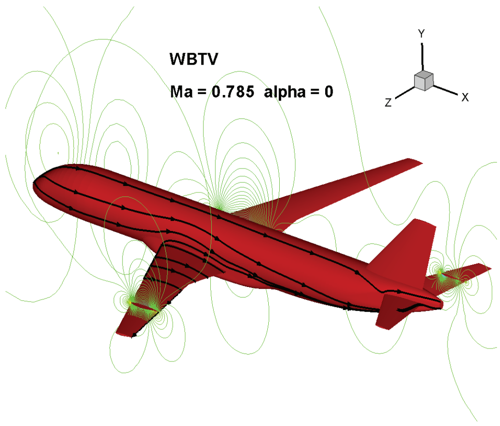

(b) Pressure contours

Figure 8: Grid skeleton and pressure contours of a transonic airplane configuration.

Usually, the implementations of high-order schemes for complex three-dimensional grids are much more difficult than that of low-order schemes as numerical oscillations and instabilities will cause the failure of high-order applications. This shortage of high-order finite difference schemes can be largely mitigated for subsonic problems by applying the CBIC and the CMM mentioned above. From the isotonic total-pressure surface and the pressure contours of the double-delta wing shown in Fig. 7, it can be found that the result is oscillation free and the main vortex core, the secondary vortex core, as well as the breakdown of the main vortex are clearly resolved. The CMM can also enhance the capability of the WCNS for complex shock wave problems. Fig. 8 shows the grid skeleton and the pressure contours of a transonic airplane configuration. Fig. 9 shows the grid

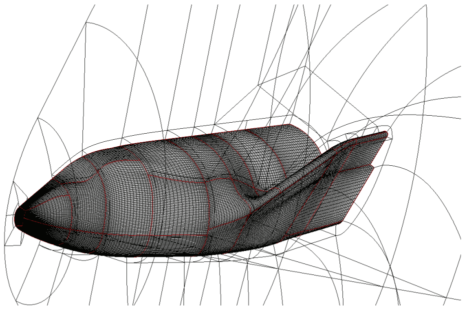

(a) Gird skeleton

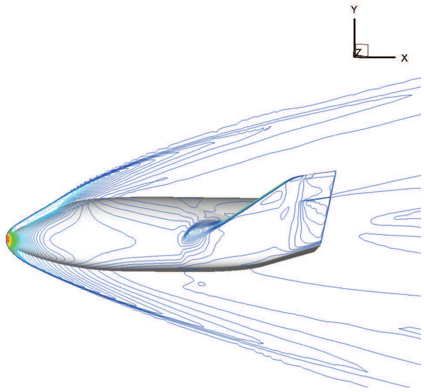

(b) $\alpha=0°$

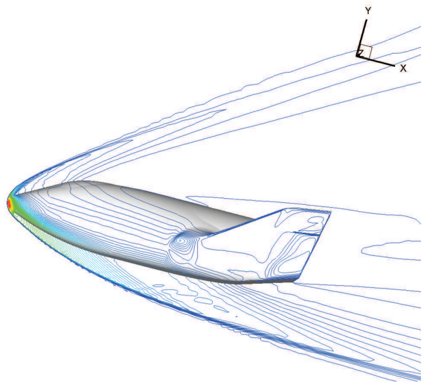

(c) $\alpha=20°$

Figure 9: Grid skeleton and pressure contours of the hypersonic X-38 configuration ($\alpha=0°$).

skeleton and the pressure contours of the hypersonic X-38 configuration. It can be seen from the two figures that the flows are smooth despite that the grids are complex with many block interfaces.

7 Concluding remarks

In contrast to the rapid development of high-order algorithms in CFD, the applications of high-order and high accurate methods on complex configurations are still limited. One of the reasons, which baffle the wide applications of high-order schemes in engineering-oriented problems, is mainly derived from the complexity of grids.

In order to apply high-order schemes for multi-block grids, the characteristic-based interface conditions (CBIC) are employed to conduct the transmission of flow information. Our results indicate that the CBIC can handle complex multi-block grids conveniently and effectively. For the purpose of satisfying the three surface conservation items of the GCL (or SCL) in discretized forms, a conservative metric method (CMM) was employed for curvilinear coordinates. The CMM, which is independent to the accuracy of a scheme, can eliminate the GCL-related errors derived from the discretization of flow fluxes, while the traditional standard metric method can cause unacceptable GCL-related errors because of discretization errors when the grid quality is low. Numerical tests demonstrate that the GCL is very important to ensure the freestream conservation, as well as to help to prevent numerical oscillations.

Finally, the successful applications of the high-order WCNS-E-5 to complex problems are briefly shown. The complex problems include a double-delta wing, a transonic airplane configuration, and a hypersonic X-38 configuration. Some other complex applications of WCNS can be found in [16, 32, 79, 97–99]. These researches show pleasant prospects in engineering-oriented applications of high-order WCNS schemes especially for detailed simulations.

Acknowledgments

This study was supported by the project of National Natural Science Foundation of China (Grant 11072259 and 10621062) and National Basic Research Program of China (Grant No. 2009CB723800). The authors would like to thank Dr. Huayong Liu, and Assistant Researcher Guangxue Wang of State Key Laboratory of Aerodynamics for their contributions.

References

[1] Wang, Z.J., High-Order Methods for the Euler and Navier-Stokes Equations on Unstructured Grids, Progress in Aerospace Sciences, 43 (2007), pp. 1-41.
[2] Shu, C.-W., High-Order Finite Difference and Finite Volume WENO Schemes and Discontinuous Gakerkin Methods for CFD, Int. J. Comput. Fluid Dyn., 17 (2003), pp. 107-118.
[3] Cheng, J., and Shu, C.-W., High Order Schemes for CFD: a Review, Chinese J. Comput. Phys., 26(5) (2009), pp. 633-655.
[4] Ekaterinaris, J.A., High-Order Accurate, Low Numerical Diffusion Methods for Aerodynamics, Progress in Aerospace Sciences, 41 (2005), pp. 192-300.

[5] Lele, S.K., Compact Finite Difference Schemes with Spectral-Like Resolution, J. Comput. Phys., 103 (1992), pp. 16-42.

[6] Deng, X., Maekawa, H., and Shen, Q., A Class of High Order Dissipative Compact Schemes, AIAA Paper, 96-1972, (1996).

[7] Visbal, M.R., and Gaitonde, D.V., High-Order Accurate Methods for Complex Unsteady Subsonic Flows, AIAA Journal, 37(10) (1999), pp. 1231-1239.

[8] Deng, X., Maekawa, H., Compact High-Order Accurate Nonlinear Schemes, J. Comput. Phys., 130 (1997), pp. 77-91.

[9] Deng, X., and Zhang, H., Developing High-Order Accurate Nonlinear Schemes, J. Comput. Phys., 165 (2000), pp. 22-44.

[10] Deng, X., High-Order Accurate Dissipative Weighted Compact Nonlinear Schemes, Science in China (Serial A), 45(3) (2002), pp. 356-370.

[11] Liu, X., Deng, X., and Mao, M., High-Order Behaviors of Weighted Compact Fifth-Order Nonlinear Schemes, AIAA Journal, 45(8) (2007), pp. 2093-2097.

[12] Sumi, T., Kurotaki, T., and Hiyama, J., Generalized Characteristic Interface Conditions with High-Order Interpolation Method, AIAA Paper, 2008-752, (2008).

[13] Gaitonde, D.V., and Visbal, M.R., Padé-Type High-Order Boundary Filters for the Navier-Stokes Equations, AIAA Journal, 18(11) (2000), pp. 2103-2112.

[14] Delf, J.W., Sound Generation From Gust-Airfoil Interaction Using CAA-Chimera Method, AIAA Paper, 2001-2136, (2001).

[15] Sherer, S.E., Gordnier, R.E., and Visbal, M.R., Computational Study of a UCAV Configuration Using a High-Order Overset-Grid Algorithm, AIAA Paper, 2008-626, (2008).

[16] Fujii, K., Nonomura, T., and Tsutsumi, S. Toward Accurate Simulation and Analysis of Strong Acoustic Wave Phenomena-A Rview Fom the Eperience of Our Study on Rocket Problems, Int. J. Numer. Meth. Fluids, 64 (2010), pp. 1412-1432.

[17] Rai, M.M., A Relaxation Approach to Patched Grid Calculations with the Euler Equations, J. Comput. Phys., 66 (1986), pp. 99-131.

[18] Lerat, A., and Wu, Z.N., Stable Conservative Multidomain Treatments for Implicit Euler Equations, J. Comput. Phys., 123 (1996), pp. 45-64.

[19] Huan, X., Hicken, J.E., and Zingg, D.W., Interface and Boundary Schemes for High-Order Methods, AIAA Paper 2009-3658, (2009).

[20] Hicken, J.E., and Zingg, D.W., Parallel Newton-Krylov Solver for the Euler Equations Discretized Using Simultaneous-Approximation Terms, AIAA Journal, 46(11) (2008), pp. 2773-2786.

[21] Kreiss, H.-O., and Scherer, G., Finite Element and Finite Difference Methods for Hyperbolic Partial Differential Equations, Mathematical Aspects of Finite Elements in Partial Differential Equations, Academic Press, New York, (1974).

[22] Mattsson, K., Boundary Procedures for Summation-by-Parts Operators, SIAM J. Sci. Comput., 18(1) (2003), pp. 133-153.

[23] Olsson, P., Summation by Parts, Projections, and Stability. I, Math. Comput., 64(211) (1995), pp. 1035-1065.

[24] Carpenter, M.H., Gottlieb, D., and Abarbanel, S., Time-Stable Boundary Conditions for Finite-Difference Schemes Solving Hyperbolic Systems, J. Comput. Phys., 111 (1994), pp. 220-236.

[25] Nordström, J. and Carpenter, M.H., Boundary and Interface Conditions for High-Order Finite-Difference Methods Applied to the Euler and Navier-Stokes Equations, J. Comput. Phys., 148 (1999), pp. 621-645.

[26] Carpenter, M.H., Nordstrom, J., and Gottlieb, D., A Stable and Conservative Interface Treatment of Arbitrary Spatial Accuracy, SIAM J. Sci. Comput., 148 (1999), pp. 341-365.

[27] Strand, B., Summation by Parts for Finite Difference Approximations for d/dx, J. Comput. Phys., 110 (1994), pp. 47-67.

[28] Jurgens, H.M. and Zingg, D.W., Numerical Solution of the Time-Domain Maxwell Equations Using High-Accuracy Finite-Difference Methods, SIAM J. Sci. Comput., 22(5) (2001), pp. 1675-1696.

[29] Kim, J.W., and Lee, D.J., Characteristic Interface Conditions for Multi-Block High-Order Computation on Singular Structured Grid, AIAA Paper, 2003-3122, (2003).

[30] Sumi, T., Kurotaki, T., and Hiyama, J., Generalized Characteristic Interface Conditions for Accurate Multi-Block Computation, AIAA Paper, 2006-1272, (2006).

[31] Sumi, T., Kurotaki. T., and Hiyama, J., Practical Multi-Block Computation with Generalized Characteristic Interface Conditions Around Complex Geometry, AIAA Paper, 2007-4471, (2007).

[32] Deng, X., Mao, M., and Tu, G., et al., Extending the fifth-order weighted compact nonlinear scheme to complex grids with characteristic-based interface conditions, AIAA Journal, 48(12) (2010), pp. 2840-2851.

[33] Fu, D., Ma, Y., Analysis of Super Compact Finite Difference Method and Application to Simulation of Vortex-Shock Interaction, Int. J. Numer. Meth. Fluids, 36(7) (2001), pp. 773-805.

[34] Uzgoren, E., Sim, J., Shyy, W., Marker-Based, 3-D Adaptive Cartesian Grid Method for Multiphase Flow Around Irregular Geometries, Commun. Comput. Phys., 5 (2009), pp. 1-41.

[35] Yee, H.C., Explicit and Implicit Multidimensional Compact High-Resolution Shock-Capturing Methods: Formulation, J. Comput. Phys., 131 (1997), pp. 216-232.

[36] Sjogreen, B., Yee, H.C., Variable High Order Multiblock Overlapping Grid Methods for Mixed Steady and Unsteady Multiscale Viscous Flows, Commun. Comput. Phys., 5 (2009), pp. 730-744.

[37] Osher, S., Efficient Implementation of High Order Accurate Essentially Non-Oscillatory Shock Capturing Algorithms Applied to Compressible Flow, Numerical Methods for Compressible Flows-Finite Difference, Element and Volume Techniques. Anaheim, Ca, UAS: ASME, New York, NY, UAS, (1986), pp. 127-128.

[38] Chakravarthy, S.R., Harten, A., and Osher, S., Essentially Non-Oscillatory Shock-Capturing Schemes of Arbitrarily-High Accuracy, AIAA-86-0339 (1986).

[39] Shu, C.-W., High Oder Weighted Essentially Non-Oscillatory Schemes for Convection Dominated Problems, SIAM Rev., 51 (2009), pp. 82-126.

[40] Cockburn, B., and Shu, C.-W., The Runge-Kutta Discontinuous Galerkin Finite Element Method for Conservation Laws V: Multidimensional Systems, J. Comput. Phys., 141 (1998), pp. 199-224.

[41] Bassi, F., and Rebay, S., Numerical Evaluation of Two Discontinuous Galerkin Methods for the Compressible Navier-Stokes Equations, Int. J. Numer. Meth. Fluids, 40(1) (2002), pp. 197-207.

[42] Dolejsi, V., Semi-Implicit Interior Penalty Discontinuous Galerkin Methods for Viscous Compressible Flows, Commun. Comput. Phys., 4 (2008), pp. 231-274.

[43] Luo, H., Baum, J.D., and Lohner, R., A Discontinous Galerkin Method Based on a Taylor Basis for the Compressible Flows on Arbitrary Grids, J. Comput. Phys., 227 (2008), pp. 8875-8893.

[44] Dumbser, M., Balsara, D.S., Toro, E.F., and Munz, C.D., A Unified Framework for the Construction of One-Sep Finite Volume and Discontinuous Galerkin Schemes on Unstructured Meshes, J. Comput. Phys., 227 (2008), pp. 8209-8253.
[45] Ferrari, A., Dumbser, M., Toro, E.F., Armanini, A., A New Stable Version of the SPH Method in Lagrangian Coordinates, Commun. Comput. Phys., 4 (2008), pp. 378-404.
[46] Grosso, G., Antuono, M., Toro, E.F., The Riemann Problem for the Dispersive Nonlinear Shallow Water Equations, Commun. Comput. Phys., 7 (2010), pp. 64-102.
[47] Dumbser, M., Toro, E.F., On Universal Osher-Type Schemes for General Nonlinear Hyperbolic Conservation Laws, Commun. Comput. Phys., 10 (2011), pp. 635-671.
[48] Wang, L., and Mavriplis, D.J., Implicit Solution of the Unsteady Euler Equations for High-Order Accurate Discontinuous Galerkin Discretiztions, J. Comput. Phys., 225 (2007), pp. 1994-2015.
[49] Nastase, C.R., and Mavriplis, D.J., High-Order Discontinuous Galerkin Methods Using a Hp-Multigrid Approach, J. Comput. Phys., 213 (2006), pp. 330-357.
[50] Abgrall, R., Shu, C.-W., Development of Residual Distribution Schemes for the Discontinuous Galerkin Method: The Scalar Case with Linear Elements, Commun. Comput. Phys., 5 (2009), pp. 376-390.
[51] Xia, Y., Xu, Y., Shu, C.-W., Application of the Local Discontinuous Galerkin Method for the Allen-Cahn/Cahn-Hilliard System, Commun. Comput. Phys., 5 (2009), 821-835.
[52] Zhang, Z.-T., Shu, C.-W., Third Order WENO Scheme on Three Dimensional Tetrahedral Meshes, Commun. Comput. Phys., 5 (2009), pp. 836-848.
[53] Zhang, R., Zhang, M., Shu, C.-W., On the Order of Accuracy and Numerical Performance of Two Classes of Finite Volume WENO Schemes, Commun. Comput. Phys., 9 (2011), pp. 807-827.
[54] Kroll, N., ADIGMA - A European Project on the Development of Adaptive Higher Order Variational Methods for Aerospace Applications, European Conference on Computational Fluid Dynamics, Eccomas CDF, (2006).
[55] Patera, A.T., A Spectral Element Method for Fluid Dynamics: Laminar Flow in a Channel Expansion, J. Comput. Phys., 54 (1984), pp. 468.
[56] Liu, Y., Vinokur, M. and Wang, Z.J., Spectral (Finite) Volume Method for Conservation Laws on Unstructured Grids V: Extension to Three-Dimensional Systems, J. Comput. Phys., 215 (2006), pp. 454-472.
[57] Sun, Y., Wang, Z.J., and Liu, Y., Spectral (finite) Volume Method for Conservation Laws on Unstructured Grids VI: Extension to Viscous Flow, J. Comput. Phys., 215 (2006), pp. 41-58.
[58] Sun, Y., Wang, Z.J., and Liu, Y., High-Order Multi-Domain Spectral Difference Method for the Navier-Stokes Equations on Unstructured Hexahedral Grids, Commun. Comput. Phys., 2(2) (2007), pp. 310-333, and also AIAA Paper 2006-301, (2006).
[59] Kitamura, K., Shima, E., Fujimoto, K., Wang, Z.J., Performance of Low-Dissipation Euler Fluxes and Preconditioned LU-SGS at Low Speeds, Commun. Comput. Phys., 10 (2011), pp. 90-119.
[60] Kopriva, D.A., A Staggered-Grid Multidomian Spectral Method for the Compressible Navier-Stokes Equations, J. Comput. Phys., 143 (1998), pp. 125-158.
[61] Xu, K., Jin, C., A Unified Moving Grid Gas-Kinetic Method in Eulerian Space for Viscous Flow Computation, J. Comput. Phys., 222 (2007), pp. 155-175.
[62] Jin, C., Xu, K., Numerical Study of the Unsteady Aerodynamics of Freely Falling Plates, Commun. Comput. Phys., 3 (2008), pp. 834-851.
[63] Xu, K., A Gas-Kinetic BGK Scheme for the Navier-Stokes Equations and its Connection

with Artificial Dissipation and Godunov Method, J. Comput. Phys., 171 (2001) 289-335.
[64] Xu, K., Liu, H., A Multiple Temperature Kinetic Model and its Application to Near Continuum Flows, Commun. Comput. Phys., 4 (2008), pp. 1069-1085.
[65] Ni, G., Jiang, S., and Xu, K. Remapping-Free ALE-Type Kinetic Method for Flow Computations, J. Comput. Phys., 228 (2009), pp. 3154-3171.
[66] Chen, Y., Jiang, S., An Optimization-Based Rezoning for ALE Methods, Commun. Comput. Phys., 4 (2008), pp. 1216-1244.
[67] Tam, C.K.W., and Webb, J.C., Dispersion-Relation-Preserving Finite Difference Schemes for Computational Acoustics, J. Comput. Phys., 107 (1993), pp. 262-281.
[68] Yee, H.C., Sandham, N. D., Hadjadj, A., Progress in the Development of a Class of Efficient Low Dissipative High Order Shock-Capturing Methods, Proceeding of the Symposium in Computational Fluid Dynamics for the 21st Century, July, (2000), Kyoto, Japan.
[69] Suresh, A., and Huynk, H.T., Accurate Monotonicity Preserving Scheme with Runge-Kutta Time Stepping, J. Comput. Phys., 136 (1997), pp. 83-99.
[70] Daru, V., and Tenaud, C., High Order One Step Monotonicity-Preserving Schemes for Unsteady Compressible Flow Calculations, J. Comput. Phys., 193, (2004), pp. 563-594.
[71] Trefethen, L.N., Group Velocity in Finite Difference Schemes, SIAM Rev., 24(2) (1982), pp. 113-136.
[72] Ma, Y., and Fu, D., Forth Order Accurate Compact Scheme with Group Velocity Control (GVC), Science in China (Serial A), 44(9) (2001), pp. 1197-1204.
[73] Ren, Y., Liu, M., and Zhang, H., A Characteristic-Wise Hybrid Compact-WENO Schemes for Solving Hyperbolic Conservations, J. Comput. Phys., 192 (2005), pp. 365-386.
[74] Adams, N.A., and Shariff, K., A High-Resolution Hybrid Compact-ENO Scheme for Shock-Turbulence Interaction Problems, J. Comput. Phys., 127 (1996), pp. 27.
[75] Pirozzoli, S., Conservative Hybrid Compact-WENO Schemes for Shock-Turbulence Interaction, J. Comput. Phys., 179 (2002), pp. 81-117.
[76] Wang, Z., and Huang, G., An Essentially Nonoscillatory High-Order Padé-Type (ENO-Padé) Scheme, J. Comput. Phys., 177 (2002), pp. 37-58.
[77] `http://aaac.larc.nasa.gov/tsab/cfdlarc/aiaa-dpw`
[78] Visbal, R.M., Gaitonde, D.V., On the Use of Higher-Order Finite-Difference Schemes on Curvilinear and Deforming Meshes, J. Comput. Phys., 181 (2002), pp. 155-185.
[79] Nonomura, N., Iizuka, N., and Fujiji, K., Freestream and Vortex Preservation Properties of High-Order WENO and WCNS on Curvilinear Grids, Comput. Fluids, 39 (2010), pp. 197-214.
[80] Trulio, J.G., and Trigger, K.R., Numerical Solution of the One-Dimensional Hydrodynamic Equations in an Arbitrary Time-Dependent Coordinate System, Technical Report UCLR-6522, University of California Lawrence Radiation laboratory, (1961).
[81] Cheng, J., Shu, C.-W., A Third Order Conservative Lagrangian Type Scheme on Curvilinear Meshes for the Compressible Euler Equations, Commun. Comput. Phys., 4 (2008), pp. 1008-1024.
[82] Qiu, J.-M., Shu, C.-W., Conservative Semi-Lagrangian Finite Difference WENO Formulations with Applications to the Vlasov Equation, Commun. Comput. Phys., 10 (2011), pp. 979-1000.
[83] Liu, W., Yuan, L., Shu, C.-W., A Conservative Modification to the Ghost Fluid Method for Compressible Multiphase Flows, Commun. Comput. Phys., 10 (2011), pp. 785-806.
[84] Pulliam, T.H., and Steger, J.L., On Implicit Finite-Difference Simulations of Three-Dimensional Flow, AIAA Paper 78-10, (1978).

[85] Thomas, P.D., and Lombard, C.K., Geometric Conservation Law and Its Application to Flow Computations on Moving Grids, AIAA Journal, 17(10) (1979), pp. 1030-1037.
[86] Étienne, S., Garon, A., and Pelletier, D., Perspective on the Geometric Conservation Law and Finite Element Methods for ALE Simulations of Incompressible Flow, J. Comput. Phys., 228 (2009), pp. 2313-2333.
[87] Bassi, F., and Rebay, S., A High-Order Accurate Discontinuous Finite Element Method for the Numerical Solution of the Compressible Navier-Stokes Equations, J. Sci. Comput., 131 (1997), pp. 267-279.
[88] Bassi, F., and Rebay, S., GMRES Discontinuous Galerkin Solution of the Compressible Navier-Stokes Equations, In Karniadakis Cockburn and Shu, eds., Discontinuous Galerkin Methods: Theory, Computation and Applications, pp. 197-208. Springer, Berlin, 2000.
[89] Thompson, K.W., Time Dependent Boundary Conditions for Hypersonic System, II, J. Comput. Phys., 89, (1990), pp. 439-461.
[90] Poinsot, T.J., and Lele, S.K., Boundary Conditions for Direction Simulations of Compressible Viscous Flows, J. Comput. Phys., 101 (1992), pp. 104-129
[91] Spalart, P.R., and Allmaras, S.R., A One-Equation Turbulence Model for Aerodynamic Flows, AIAA Paper 92-0439, (1992).
[92] Zhang, H., and Zhuang, F., NND Schemes and Their Applications to Numerical Simulation of Two- and Three-Dimensional Flows, Adv. Appl. Mech., 29 (1991), pp. 193-256
[93] Zhang, H., Reggio, M., Trépanier, J. Y., Camarero, R.,Discrete Form of the GCL for Moving Meshes and its Implementation in CFD Shemes, Comput. Fluids, 22 (1993), pp. 9-23.
[94] Tu, G., Deng, X., Mao, M., A Staggered Non-Oscillatory Finite Difference Method for High-Order Discretization of Viscous Terms, Acta Aerodynamica Sinica, 29(1) (2011), pp. 10-15.
[95] Wieting, A. R., Experimental Study of Shock Wave Interference Heating on a Cylindrical Leading Edge, NASA TM-100484, (1987).
[96] Fujii, K. Progress and Future Prospects of CFD in Aerospace-Wind Tunnel and Beyond, Progress in Aerospace Sciences, 41 (2005), pp. 455-470.
[97] Fujii, K. CFD Contributions to High-Speed Shock-Related Problems: Examples Today and New Features Tomorrow, Shock Waves, 18 (2008), pp. 145-154.
[98] Ishiko, K., Ohnishi, N., Ueno, K., et al., Implicit Large Eddy Simulation of Two-Dimensional Homogeneous Turbulence Using Weighted Compact Nonlinear Scheme, J. Fluid Eng., 131(6) (2009), pp. 1-14.
[99] Deng, X., Liu, X., Mao, M. et al., Advances in High-Order Accurate Weighted Compact Nonlinear Schemes. Adv. Mech., 37(3) (2007), pp.417-427.
[100] Deng, X., Mao, M., Tu, G., et al., Geometric Conservation Law and Applications to High-Order Finite Difference Schemes with Stationary Grids, J. Comput. Phys., 230(4) (2011), pp. 1100-1115.
[101] Shen, Y., Zha, G., and Chen, X., High Order Conservative Differencing for Viscous Terms and the Application to Vortex-Induced Vibration Flows, J. Comput. Phys., 228 (2009), pp. 8283-8300.
[102] Kannan, R., and Wang, Z.J., A Study of Viscous Flux Formulations for a p-Multigrid Spectral Volume Navier Stokes Solver, J. Sci. Comput., 41(2) (2009), pp. 165-199.
[103] Kannan, R., and Wang, Z.J., LDG2: A Variant of the LDG Flux Formulation for the Spectral Volume Method, J. Sci. Comput., 46(2) (2010), pp. 314-328.
[104] Kannan, R., and Wang, Z.J., The Direct Discontinuous Galerkin (DDG) Viscous Flux Scheme for the High Order Spectral Volume Method, Comput. Fluids, 39(10) (2010), pp. 2007-2021

[105] Sun, Y., Wang, Z.J., Liu, Y., Spectral (Finite) Volume Method for Conservation Laws on Unstructured Grids VI: Extension to Viscous Flow, J. Comput. Phys., 215 (2006), pp. 41-58.
[106] Zhang, Y., Deng, X., Mao, M. et al., Investigation of Convergence Acceleration for High-Order Scheme (WCNS) in 2D Supersonic Flows, Acta Aerodynamica Sinica, 26(1) (2008), pp. 14-18.
[107] Parsani, M., Ghorbaniasl, G., Lacor, C., et al., An Implicit High-Order Spectral Difference Approach for Large Eddy Simulation, J. Comput. Phys., 229(14) (2010), pp. 5373-5393.
[108] Kannan, R., An implicit LU-SGS Spectral Volume Method for the Moment Models in Device Simulations: Formulation in 1D and Application to A P-Multigrid Algorithm, Int. J. Numer. Methods Biomed. Eng., (Article online in advance of print) n/a. doi: 10.1002/cnm.1359.
[109] Sun, Y., Wang, Z.J., Liu, Y., Efficient Implicit Non-linear LU-SGS Approach for Compressible Flow Computation Using High-Order Spectral Difference Method, Commun. Comput. Phys., 5 (2009), pp. 760-778.
[110] Haga, T., Sawada, K., Wang, Z.J., An Implicit LU-SGS Scheme for the Spectral Volume Method on Unstructured Tetrahedral Grids, Commun. Comput. Phys., 6 (2009), pp. 978-996.
[111] Luo, H., Baum, J. D., Löhner, R., A P-Multigrid Discontinuous Galerkin Method for the Euler Equations on Unstructured Grids, J. Comput. Phys., 211 (2006), pp. 767-783.
[112] Fidkowski, K.J., Oliver, T.A., Lu, J., et al., P-Multigrid Solution of High-Order Discontinuous Galerkin Discretizations of the Compressible Navier-Stokes Equations, J. Comput. Phys., 207 (2005), pp. 92-113.
[113] Liang, C., Kannan, R., Wang, Z.J., A P-Multigrid Spectral Difference Method with Explicit and Implicit Smoothers on Unstructured Triangular Grids, Comput. Fluids, 38(2) (2009), pp. 254-265.
[114] Ronquist, E.M., Patera, A.T., Spectral Element Multigrid, I. Formulation and Numerical Results, J. Sci. Comput., 2(4) (1987), pp. 389-406.